# Speckle Engineering through Singular Value Decomposition of the Transmission Matrix

Louisiane Devaud,[1,*] Bernhard Rauer,[1] Jakob Melchard,[2] Matthias Kühmayer,[2] Stefan Rotter,[2] and Sylvain Gigan[1]

[1]*Laboratoire Kastler Brossel, ENS-Université PSL, CNRS, Sorbonne Université, Collège de France, 24 rue Lhomond, 75005 Paris, France*

[2]*Institute for Theoretical Physics, Vienna University of Technology (TU Wien), A-1040 Vienna, Austria*

(Received 1 December 2020; accepted 14 July 2021; published 27 August 2021)

Speckle patterns are ubiquitous in optics and have multiple applications for which the control of their spatial correlations is essential. Here, we report on a method to engineer speckle correlations behind a scattering medium through the singular value decomposition of the transmission matrix. We not only demonstrate control over the speckle grain size and shape but also realize patterns with nonlocal correlations. Moreover, we show that the reach of our method extends also along the axial dimension, allowing volumetric speckle engineering behind scattering layers.

DOI: 10.1103/PhysRevLett.127.093903

Speckle formation is a universal feature of coherent wave dynamics in disordered systems. It occurs whenever the phase front of a wave is randomly perturbed. Particularly in optics, this phenomenon gathered considerable interest, for both its fundamental aspects and its technological applications. Although fully developed speckle patterns are inherently random, they exhibit predictable properties [1]. Their field amplitudes follow a Rayleigh distribution, while spatially they are correlated only locally. The spatial extent of these local correlations is usually referred to as the speckle grain size. These universal features make speckle patterns a valuable tool for imaging techniques [2–4], optical tweezers [5,6], or random potentials for cold atoms [7,8]. For all these applications, being able to tune the speckle patterns' properties is highly desirable and would provide valuable degrees of control.

Recently, several methods have been developed to tailor the properties of speckle patterns. They range from approaches to alter the patterns' statistics [9,10] to others that target their spatial correlations [11–14]. While the former allow for nearly arbitrary intensity distributions to be realized, the latter focus mainly on single correlation features with limited flexibility. More versatile techniques, such as in Ref. [15], concentrate only on intensity correlations and demand for an iterative procedure to arrive at the desired pattern. Also, they act on a single axial plane and, therefore, cannot alter axial correlations. More flexible and direct methods to customize the correlations in speckle patterns are, therefore, highly desirable.

In this Letter, we strike a new path for engineering the spatial correlations of speckle patterns, utilizing a spatial light modulator (SLM) and a multiple scattering medium. Our approach not only enables the volumetric control of the size and shape of the speckle grains after the medium but also allows one to imprint nonlocal correlations. To achieve this control, we leverage the concept of the transmission matrix (TM) and its singular value decomposition (SVD). The TM is a powerful tool that encodes the relation between input and output modes of the scattering medium, allowing one to focus light or transmit images at its output [16–18]. Its SVD, a generalization of the eigendecomposition to nonsquare matrices, can be used for selective focusing [19–21], to identify open and closed channels [22–25], or to find dispersion-free states from the spectral variation of the TM [26,27]. Here, we show that, for spatially oversampled TMs that capture the local speckle correlations, the SVD also provides indirect control of these spatial correlations. Consider, for example, a situation where field components of low spatial frequencies are more strongly transmitted through the medium. In that case, the first singular vector, with the highest transmission, will preferentially select these slowly varying components, leading to an enlarged speckle grain size. More generally, the full spectrum of singular vectors facilitates a flexible and customized control of the grain size. We show further that purely computational Fourier filtering of the TM can be used to achieve arbitrary correlations, from asymmetric speckle grains to nonlocal correlations and Bessel-like speckle patterns. Moreover, the control obtained through the SVD extends also to the axial direction, going beyond the reach of established methods.

Our experimental setup is presented in Fig. 1. The wave front of a coherent light source is modulated by an SLM before being focused on a layer of scattering material. The scattered light that is transmitted through the medium forms a speckle pattern imaged onto a camera. Over a second path, an unperturbed plane wave, decoupled from the beam before the SLM, is recombined and interferes with the scattered light at the CCD. This configuration enables the measurement of the complex light field after the medium

 

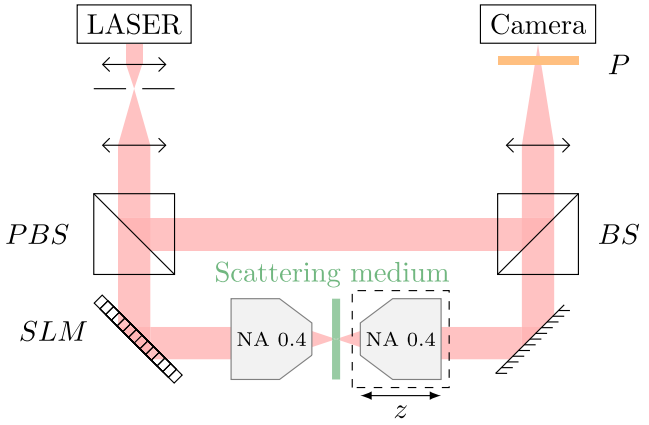


FIG. 1. Experimental scheme. A beam delivered from a Ti: sapphire laser (MaiTai HP, Spectra-Physics) is divided into two paths by a polarizing beam splitter (PBS). On one path, the wave front is modulated by a reflective phase-only SLM (HSP512L-1064, Meadowlarks). This modulated light is focused on a layer of scattering material ($TiO_2$ layer suspended on a glass slide, thickness of $\sim 10$ $\mu$m resulting in a transmittance of $\simeq 0.3$) by an imaging objective with a numerical aperture (NA) of 0.4 (Olympus PLN20X). An identical second objective is used to image the transmitted scattered light onto a charged coupled device (CCD) camera (Manta G-046B, Allied Vision). The second objective is mounted on a translational stage allowing one to image the transmitted light at varying distances $z$ from the medium. The two paths are recombined on a beam splitter (BS). A polarizer ($P$) in front of the camera ensures that only light with a selected polarization is measured.

through digital phase-stepping holography. The polarization of the reference path is chosen to be orthogonal to the one of the light sent onto the diffusive medium, ensuring that only multiply scattered light is detected in the interferogram [28]. The TM is constructed by displaying a basis of input patterns on the SLM and recording the corresponding output fields [16].

We first measure the TM at a distance of 1 mm behind the medium output surface (see [29], Sec. I). In order to capture the local correlations of the light field in the TM measurement, we spatially oversample the imaged speckle patterns (i.e., a single speckle grain covers several camera pixels). Performing the SVD of the measured TM gives access to the sorted singular values and associated singular vectors. We send one of these vectors through the medium by applying its phase as a modulation on the SLM. To study how the speckle grain size depends on the singular vector chosen, we record the light field at the image plane. Figure 2(a) shows the observed speckle patterns for three different singular vectors together with a reference speckle obtained when displaying a blank pattern on the SLM. The first singular vector (No. 1), associated to the largest transmission, leads to an enlarged speckle grain size, corresponding to a narrower $k$ distribution in Fourier space compared to the reference. An intermediate vector (No. 81), leads to a grain size smaller than the reference, while the last vector (No. 225) results in a speckle that is indistinguishable from a random input state. In Fourier space, increasing the vector number leads to the appearance of a ring with growing radius and decreasing amplitude (for the last vectors, the ring fades completely). Similar effects of ring-shaped distributions of light in real space have been observed for the SVD of an acousto-optic TM [30].

To quantitatively compare the speckle grain size for different inputs, we calculate the output pattern's autocorrelation and extract its full width at half maximum (FWHM). Figure 2(b) shows the speckle grain size over the singular vector number, relative to the size of the reference speckles. The first singular vectors lead to a grain size increase, whereas the intermediate ones result in a decrease, as observed in Fig. 2(a). Selecting the singular vector number within this range, therefore, allows one to choose patterns with a desired grain size. The last singular vectors display a continuous transition back to the reference grain size. The change in grain size is accompanied by a change in overall transmission [Fig. 2(b), inset], as expected for the singular vectors [23].

The above experimental observations can be understood from the speckle Fourier space distribution obtained for the blank reference input [Fig. 2(a)]. There, we see that the distribution is peaked around $|\vec{k}| = 0$, meaning that spatial modes with small transverse frequency components are transmitted better than high-frequency ones. As the SVD returns the eigenmodes of the TM associated to specific values of transmission, it also results in a specificity in spatial frequency. The highly transmitting first singular vectors concentrate light in the low-frequency spatial modes, resulting in larger grains. For the less transmitting singular vectors, the opposite is happening, leading to a suppression of low-frequency components, smaller speckle grains, and the ring-shaped distributions observed in Fig. 2(a). A model based only on a random TM with local Gaussian correlations enables one to well reproduce the experimental results (see [29], Sec. II). The only condition for frequency selectivity to appear is the nonflatness of the output Fourier distribution.

Interestingly, the control gained over the local correlations of the output patterns does not substantially influence their statistics. Figure 2(c) shows the field statistics of the three example vectors shown in Fig. 2(a). In general, the field amplitudes retain their Rayleigh distribution and the phases are uniformly distributed, as expected for fully developed speckles patterns [Fig. 2(c), inset]. Only the first singular vector shows small deviations in its amplitude distribution. We attribute these to the high concentration of light in the forward scattering component with $|\vec{k}| = 0$, as, for some realizations, a preferred phase can be observed (see [29], Sec. III).

An important ingredient for the successful control of the grain size is the nonflatness of the speckle's spatial

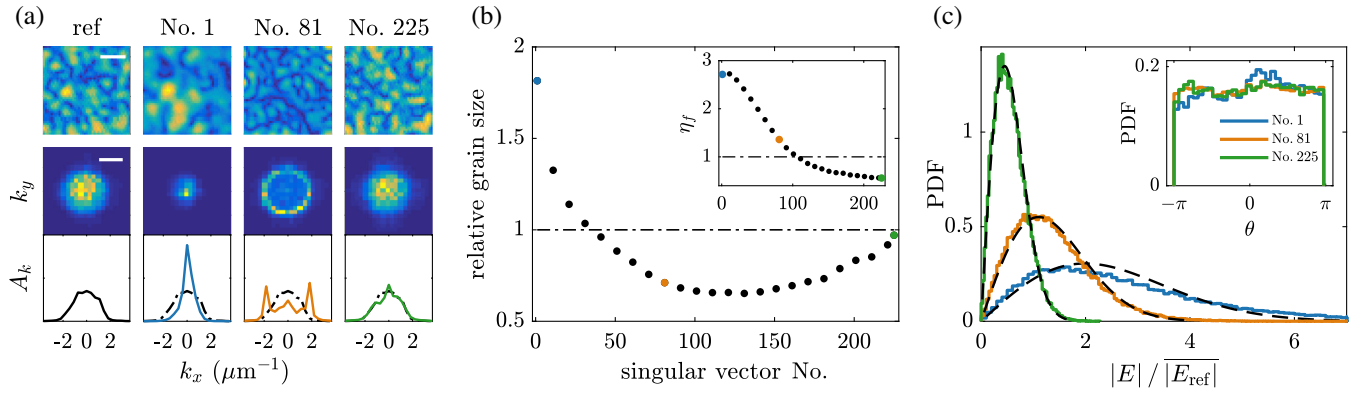


FIG. 2. Speckle grain size control through the SVD of the TM. (a) Speckle patterns obtained from displaying a blank reference pattern (ref) and three different singular vectors of the TM (No. 1, No. 81, and No. 225, out of 225). The first row shows examples of the observed field amplitude patterns in real space, while the second row displays the respective Fourier space distributions (scale bars, 5 $\mu$m and 2 $\mu$m$^{-1}$, respectively). The third row shows central cuts through these Fourier space distributions (blue, orange, and green lines) compared to the reference (black). The cuts are averaged over three pixel rows. For all panels, the data are individually normalized and do not reflect the changes in total transmission. (b) Relative speckle grain size as a function of the singular vector number (reference grain size 2 $\mu$m). The inset plots the enhancement of the field amplitude with respect to the blank reference $\eta_f$ for the different singular vectors. The dot-dashed black lines represent the mean reference values. The data points corresponding to the examples shown in (a) are marked with their respective colors (blue, orange, and green). (c) Probability density functions (PDF) of the field amplitudes obtained for the three singular vectors displayed in (a). All distributions are normalized to the average field amplitude of the reference $\overline{|E_{\mathrm{ref}}|}$ and fitted with Rayleigh distributions (dashed black lines). The inset shows the corresponding phase distributions. All results, except for speckle patterns in (a), are averaged over 36 realizations of the disorder.

frequency distribution for a random input. In our case, the limited surface area at which light exits the medium naturally leads to a peaked distribution when imaging a plane at a distance from the surface [1]. This becomes clear when picturing the limiting case of imaging a plane far removed from the medium. There, the exit surface would act like a point source, and all light would converge to the $k = 0$ mode (see [29], Sec. I). If, instead, we image the speckles right at the medium output, the collected $k$ vectors are mainly limited by the imaging NA, leading to a uniform distribution of spatial frequencies, as shown in Fig. 3(a). In such a situation, the singular vectors show no dispersion in grain size.

A convenient way to overcome such limitations is to artificially introduce the nonflatness in the spatial frequency distribution. This can be done by employing the approach developed in Ref. [31], where Fourier filtering of the TM was used to shape the point spread function when focusing light behind a medium. A TM is experimentally measured, and its output dimension is Fourier transformed and multiplied with a filter mask that introduces the desired variation from the flat distribution. After transforming it back to real space, the SVD of this filtered TM can be performed. Note that this is a fully computational procedure and no changes to the scattering medium nor to the measurement configuration are necessary (see [29], Sec. IV).

The large flexibility of the filtering process provides a wide range of control over the speckle correlations. Figures 3(b) and (c) show the results of two masks showcasing the potential of this approach. The first mask filters the high-$k_y$ components without modifying the $k_x$ components [Fig. 3(b)]. This results in a speckle pattern where grains are elongated along $y$ while their extension in $x$ remains unchanged (for a different method to achieve this asymmetry, see [29], Sec. V). The second mask selects only a specific $|k_x|$ range leading to two symmetric stripes in Fourier space [Fig. 3(c)]. Correspondingly, the speckles exhibit a short-range periodicity. The filtering approach thus enables one not only to shape the speckle grains almost arbitrarily but also to imprint nonlocal correlations on them.

A particularly interesting application is to realize speckles with a Bessel-shaped autocorrelation. For that, spatial frequencies need to be concentrated on a ring, as for regular Bessel beams [32]. The latter gathered considerable interest due to their nondiffractive nature, and several techniques were developed to generate Bessel beams behind scattering media [13,31,33]. Bessel speckle patterns, on the other hand, remain little studied, although their enhanced depth of field could be advantageous in structured illumination microscopy or speckled optical potentials [34].

To experimentally realize a Bessel speckle pattern, we first measure the TM at an arbitrary position $z_0$ behind the medium and apply the filtering technique using a ring-shaped mask. This provides us with a filtered TM that encodes only the transmission of spatial frequencies of a certain absolute value $|\vec{k}|$. As before, we perform the SVD of this filtered TM and display the phase of the first singular vector on the SLM. To verify the Bessel-like characteristics of the generated speckles, we record their axial features by

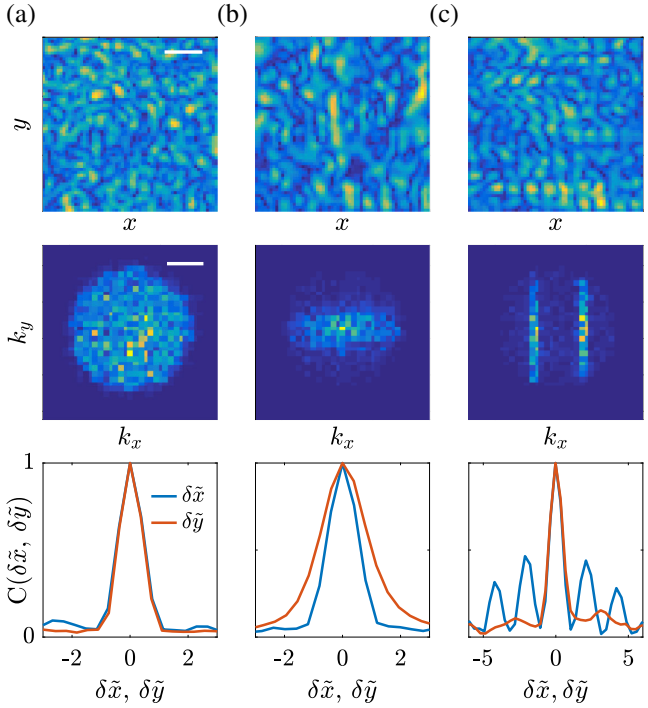


FIG. 3. Speckle engineering through the SVD of computationally filtered TMs with initially uniform spatial distribution, imaged at the output plane of the medium. (a) Reference amplitude speckle (blank SLM input). (b) Amplitude speckle obtained from displaying the first singular vector of a TM computationally filtered by a line-shaped Fourier mask. (c) The same for a TM filtered by two vertical lines selecting a specific $|k_x|$ range in Fourier space. The first row shows a single realization of the speckle pattern, while the second row shows the distribution in Fourier space (scale bars, 5 $\mu$m and 2 $\mu$m$^{-1}$, respectively; initial grain size 1.4 $\mu$m). The third row shows the autocorrelation function $C(\delta x) = |\langle E^*(x)E(x+\delta x)\rangle / \langle |E(x)|^2\rangle|$ along both the $x$ (blue) and $y$ (red) directions. The horizontal axis is rescaled by the FWHM of the reference speckle autocorrelation $w_{\mathrm{ref}}$, with $\delta\tilde{x} = \delta x / w_{\mathrm{ref}}$. The Fourier distributions as well as the autocorrelations represent an average over four disorder realizations.

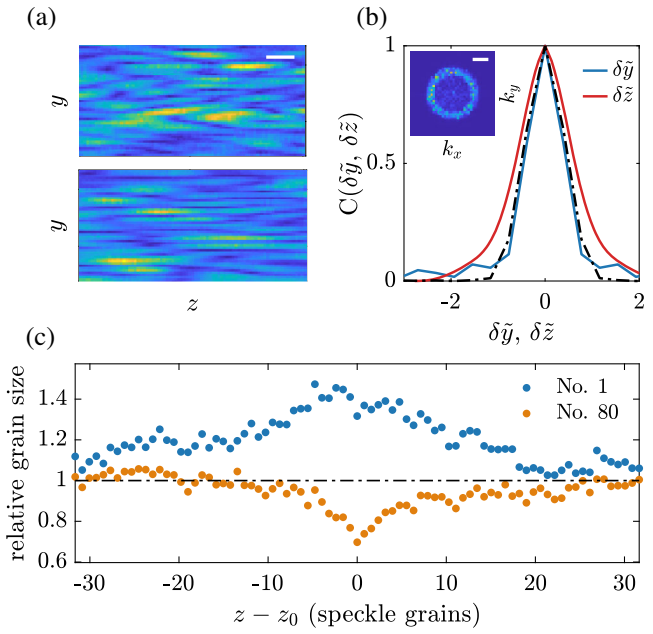


FIG. 4. Speckle correlation control along the axial dimension. (a) Reference amplitude speckle pattern (top) and output obtained for the first singular vector of a ring-filtered TM aimed at creating a Bessel speckle pattern (bottom). Both show cuts in the $(y, z)$ plane for an arbitrary $x$ position (scale bar, 5 $\mu$m). (b) Plot of the autocorrelation $C$ in $y$ (blue) and $z$ (red) direction for the first singular vector of a ring-filtered TM. Again, for both curves, the horizontal axis is rescaled by the FWHM of the reference autocorrelation along the respective dimensions (see Fig. 3). The dash-dotted black line indicates the reference autocorrelation (along $y$, equivalent to the one along $z$ due to the rescaling) obtained from a blank input. Autocorrelation data are averaged over all $x$ positions. The inset shows the corresponding Fourier space distributions in the $(x, y)$ plane at the position $z_0$ (scale bar, 2 $\mu$m$^{-1}$). (c) Relative transverse speckle grain size along the axial dimension $z$ for data taken under similar conditions as in Fig. 2. Shown are the first singular vector (No. 1, blue) and an intermediate one (No. 80, orange). The $z$ axis is rescaled by the axial extension of the reference speckle at $z_0$, where the TM was measured (12 $\mu$m). Note that the diffraction-induced increase of the speckle grain size with $z$ is not visible here, as only values relative to the local reference grain size are given.

measuring the speckled light field while scanning the positions $z$ of the imaged plane around $z_0$, providing a volumetric measurement of the output field.

The results are presented in Figs. 4(a) and 4(b), where we observe that the axial extension of the speckle grains indeed increases. Along the transverse directions, the limited spatial resolution prevents us from observing a full Bessel-shaped autocorrelation. Yet, a slight decrease in width can be qualitatively observed, and the spatial frequencies of the output patterns indeed show the desired concentration on a ring.

This result is particularly interesting, as it shows that our method allows one to control the speckle grain size in all three spatial dimensions. Even at planes away from where the TM was measured, spatial correlations are affected. Since our method does not rely on interference, changes in spatial correlations do not depend on a complicated superposition of modes that align properly only in a single plane.

Correspondingly, the ring in Fourier space selected by the first singular vector [Fig. 4(b), inset] remains visible over several axial grains, and the speckle grain modulations presented earlier persist over a large volume. Figure 4(c) shows the relative transverse grain size along the axial dimension $z$, measured under similar conditions as the data in Fig. 2. For the first singular vector, we observe the grain size enhancement over a range of about 20 axial grains. In case of the intermediate singular vector, the axial range of control is smaller but still extends beyond a few grains in the $z$ direction. These observations reach significantly

beyond [15] where the customization of speckle correlations is valid in a single plane only.

In conclusion, we experimentally demonstrate a novel method to engineer speckle correlations behind scattering media. We show how the SVD of a TM with local correlations leads to a dispersion of singular modes with respect to the output speckle grain size if the initial transmission of spatial frequencies is nonuniform. Fourier filtering of the TM can further be used to achieve arbitrary spatial mode distributions, enabling asymmetric speckle grains, nonlocal correlations, or Bessel-like speckle patterns. The filtering even lifts the requirement of oversampling the TM, facilitating its practical application. Note that the range of control obtained for the speckle correlations depends on the number of input modes controlled at the SLM compared to the region-of-interest size at the output. While the experiments discussed here have been realized on small regions of 100–400 grains, they can be scaled up by increasing the number of controlled modes (see [29], Sec. VI). Compared to previous approaches, our method proves to be more flexible and achieves a larger axial range of control. Possible applications range from structured illumination microscopy to the engineering of optical random potentials or algorithmic advantages in computational imaging [35,36]. Moreover, on a fundamental level, the principle of SVD-based control can be translated to other platforms that employ matrices encoding input-output relations as in acoustics [37] or in integrated photonic circuits [38].

We thank Michał Dąbrowski, Lorenzo Valzania, Antoine Boniface, Julien Guilbert, Jonathan Dong, and Gianni Jacucci for the careful reading of the manuscript. This project was funding by the European Research Council under Grant Agreement No. 724473 (SMARTIES), the European Union's Horizon 2020 research and innovation program under the Marie Skłodowska-Curie Grant Agreement No. 888707 (DEEP3P), and the Austrian Science Fund (FWF) under Project No. P32300 (WAVELAND).

*louisiane.devaud@lkb.ens.fr

[1] J. Goodman, *Speckle Phenomena in Optics: Theory and Applications* (Roberts & Company, Englewood, 2007).
[2] D. Lim, K. K. Chu, and J. Mertz, Wide-field fluorescence sectioning with hybrid speckle and uniform-illumination microscopy, Opt. Lett. **33**, 1819 (2008).
[3] E. Mudry, K. Belkebir, J. Girard, J. Savatier, E. Le Moal, C. Nicoletti, M. Allain, and A. Sentenac, Structured illumination microscopy using unknown speckle patterns, Nat. Photonics **6**, 312 (2012).
[4] J. Gateau, T. Chaigne, O. Katz, S. Gigan, and E. Bossy, Improving visibility in photoacoustic imaging using dynamic speckle illumination, Opt. Lett. **38**, 5188 (2013).
[5] K. M. Douglass, S. Sukhov, and A. Dogariu, Superdiffusion in optically controlled active media, Nat. Photonics **6**, 834 (2012).
[6] G. Volpe, L. Kurz, A. Callegari, G. Volpe, and S. Gigan, Speckle optical tweezers: Micromanipulation with random light fields, Opt. Express **22**, 18159 (2014).
[7] J. E. Lye, L. Fallani, M. Modugno, D. S. Wiersma, C. Fort, and M. Inguscio, Bose-Einstein Condensate in a Random Potential, Phys. Rev. Lett. **95**, 070401 (2005).
[8] J. Billy, V. Josse, Z. Zuo, A. Bernard, B. Hambrecht, P. Lugan, D. Clément, L. Sanchez-Palencia, P. Bouyer, and A. Aspect, Direct observation of Anderson localization of matter waves in a controlled disorder, Nature (London) **453**, 891 (2008).
[9] Y. Bromberg and H. Cao, Generating Non-Rayleigh Speckles with Tailored Intensity Statistics, Phys. Rev. Lett. **112**, 213904 (2014).
[10] N. Bender, H. Yılmaz, Y. Bromberg, and H. Cao, Customizing speckle intensity statistics, Optica **5**, 595 (2018).
[11] R. Fischer, I. Vidal, D. Gilboa, R. R. B. Correia, A. C. Ribeiro-Teixeira, S. D. Prado, J. Hickman, and Y. Silberberg, Light with Tunable Non-Markovian Phase Imprint, Phys. Rev. Lett. **115**, 073901 (2015).
[12] M. Guillon, B. C. Forget, A. J. Foust, V. De Sars, M. Ritsch-Marte, and V. Emiliani, Vortex-free phase profiles for uniform patterning with computer-generated holography, Opt. Express **25**, 12640 (2017).
[13] D. Di Battista, D. Ancora, M. Leonetti, and G. Zacharakis, Tailoring non-diffractive beams from amorphous light speckles, Appl. Phys. Lett. **109**, 121110 (2016).
[14] D. Di Battista, D. Ancora, G. Zacharakis, G. Ruocco, and M. Leonetti, Hyperuniformity in amorphous speckle patterns, Opt. Express **26**, 15594 (2018).
[15] N. Bender, H. Yılmaz, Y. Bromberg, and H. Cao, Introducing non-local correlations into laser speckles, Opt. Express **27**, 6057 (2019).
[16] S. M. Popoff, G. Lerosey, R. Carminati, M. Fink, A. C. Boccara, and S. Gigan, Measuring the Transmission Matrix in Optics: An Approach to the Study and Control of Light Propagation in Disordered Media, Phys. Rev. Lett. **104**, 100601 (2010).
[17] S. Popoff, G. Lerosey, M. Fink, A. C. Boccara, and S. Gigan, Image transmission through an opaque material, Nat. Commun. **1**, 81 (2010).
[18] S. Rotter and S. Gigan, Light fields in complex media: Mesoscopic scattering meets wave control, Rev. Mod. Phys. **89**, 015005 (2017).
[19] S. M. Popoff, A. Aubry, G. Lerosey, M. Fink, A. C. Boccara, and S. Gigan, Exploiting the Time-Reversal Operator for Adaptive Optics, Selective Focusing, and Scattering Pattern Analysis, Phys. Rev. Lett. **107**, 263901 (2011).
[20] T. Chaigne, O. Katz, A. C. Boccara, M. Fink, E. Bossy, and S. Gigan, Controlling light in scattering media non-invasively using the photoacoustic transmission matrix, Nat. Photonics **8**, 58 (2014).
[21] S. Jeong, Y.-R. Lee, W. Choi, S. Kang, J. H. Hong, J.-S. Park, Y.-S. Lim, H.-G. Park, and W. Choi, Focusing of light energy inside a scattering medium by controlling the time-gated multiple light scattering, Nat. Photonics **12**, 277 (2018).

[22] I. M. Vellekoop and A. P. Mosk, Universal Optimal Transmission of Light through Disordered Materials, Phys. Rev. Lett. **101**, 120601 (2008).
[23] M. Kim, Y. Choi, C. Yoon, W. Choi, J. Kim, Q.-H. Park, and W. Choi, Maximal energy transport through disordered media with the implementation of transmission eigenchannels, Nat. Photonics **6**, 581 (2012).
[24] H. Yu, T. R. Hillman, W. Choi, J. O. Lee, M. S. Feld, R. R. Dasari, and Y. K. Park, Measuring Large Optical Transmission Matrices of Disordered Media, Phys. Rev. Lett. **111**, 153902 (2013).
[25] D. Akbulut, T. Strudley, J. Bertolotti, E. P. A. M. Bakkers, A. Lagendijk, O. L. Muskens, W. L. Vos, and A. P. Mosk, Optical transmission matrix as a probe of the photonic strength, Phys. Rev. A **94**, 043817 (2016).
[26] W. Xiong, P. Ambichl, Y. Bromberg, B. Redding, S. Rotter, and H. Cao, Spatiotemporal Control of Light Transmission through a Multimode Fiber with Strong Mode Coupling, Phys. Rev. Lett. **117**, 053901 (2016).
[27] P. Ambichl, W. Xiong, Y. Bromberg, B. Redding, H. Cao, and S. Rotter, Super- and Anti-Principal-Modes in Multimode Waveguides, Phys. Rev. X **7**, 041053 (2017).
[28] M. Xu and R. R. Alfano, Random Walk of Polarized Light in Turbid Media, Phys. Rev. Lett. **95**, 213901 (2005).
[29] See Supplemental Material at http://link.aps.org/supplemental/10.1103/PhysRevLett.127.093903 which includes simulation results, the filtering technique details, an alternative method to elongate the speckle grain size, subtleties on the speckle statistics, and the evolution of the speckle spatial frequencies for different imaging planes.
[30] O. Katz, F. Ramaz, S. Gigan, and M. Fink, Controlling light in complex media beyond the acoustic diffraction-limit using the acousto-optic transmission matrix, Nat. Commun. **10**, 717 (2019).
[31] A. Boniface, M. Mounaix, B. Blochet, R. Piestun, and S. Gigan, Transmission-matrix-based point-spread-function engineering through a complex medium, Optica **4**, 54 (2017).
[32] D. McGloin and K. Dholakia, Bessel beams: Diffraction in a new light, Contemp. Phys. **46**, 15 (2005).
[33] D. Di Battista, G. Zacharakis, and M. Leonetti, Enhanced adaptive focusing through semi-transparent media, Sci. Rep. **5**, 17406 (2015).
[34] T. Schwartz, G. Bartal, S. Fishman, and M. Segev, Transport and Anderson localization in disordered two-dimensional photonic lattices, Nature (London) **446**, 52 (2007).
[35] M. Chen, E. Li, and S. Han, Application of multi-correlation-scale measurement matrices in ghost imaging via sparsity constraints, Appl. Opt. **53**, 2924 (2014).
[36] X. Wang, Y. Tao, F. Yang, and Y. Zhang, An effective compressive computational ghost imaging with hybrid speckle pattern, Opt. Commun. **454**, 124470 (2020).
[37] A. Aubry and A. Derode, Random Matrix Theory Applied to Acoustic Backscattering and Imaging in Complex Media, Phys. Rev. Lett. **102**, 084301 (2009).
[38] S. Mingaleev and K. Busch, Scattering matrix approach to large-scale photonic crystal circuits, in *Physics, Chemistry And Application Of Nanostructures*, Reviews and Short Notes to Nanomeeting 2003 (World Scientific, Singapore, 2003), pp. 59–63.